Supporting information for

Chemical dissolution pathways of MoS_2 nanosheets in biological and environmental media

Zhongying Wang[1], Annette von dem Bussche[2], Yang Qiu[1], Thomas M. Valentin[1], Kyle Gion[1], Agnes B. Kane[2, 3], Robert H. Hurt[1, 3*]

[1]School of Engineering, [2]Department of Pathology and Laboratory Medicine, [3]Institute for Molecular and Nanoscale Innovation,
Brown University, Providence, Rhode Island 02912

Contents

Text S1 Supplementary experimental section

Preparation and characterization of 2D MoS_2 nanosheets. In a typical preparation, 3 ml of 1.6 M n-butyllithium in hexane solution were added to 300 mg of MoS_2 powder (< 2 μm, Aldrich), and the mixture was left under mild stirring at room temperature for 2 days in a nitrogen-filled glovebox. The resulting lithium-intercalated product was rinsed with hexane twice to remove the excess organo-lithium reagent and organic by-products. The purified intercalated product was immediately exfoliated by reaction with DI water in an ultrasonic bath for one hour. Well-dispersed aqueous dispersion of MoS_2 nanosheets can be obtained by centrifugation at 500 rpm for 10 min to remove un-exfoliated MoS_2 materials. The byproduct LiOH was removed from the dispersion by dialysis against DI water until neutral pH. The total Mo concentration was determined by digestion with HNO_3/H_2O_2 followed by measurements in JY 2000 Ultrace ICP-AES. Dispersions of ce-MoS_2 samples were stored in a nitrogen-filled glove box. To prepare me-MoS_2 nanosheets, 100 mg MoS_2 bulk powder was added into 100 mL 2 % sodium cholate and subject to probe sonication for 5 hours. The suspension was then centrifuged at 1000 rpm for 10 min and the supernatant was collected for characterization and subsequent studies. Materials characterization was carried out using atomic force microscopy (Asylum MFP-3D Origin AFM) in pulse mode, field emission SEM (LEO 1530 VP), and high-resolution scanning transition electron microscopy (JEOL 2100F). XPS surface scans were performed on various samples using a Thermo Scientific K-Alpha XPS. Survey scans were averaged over 20 runs.

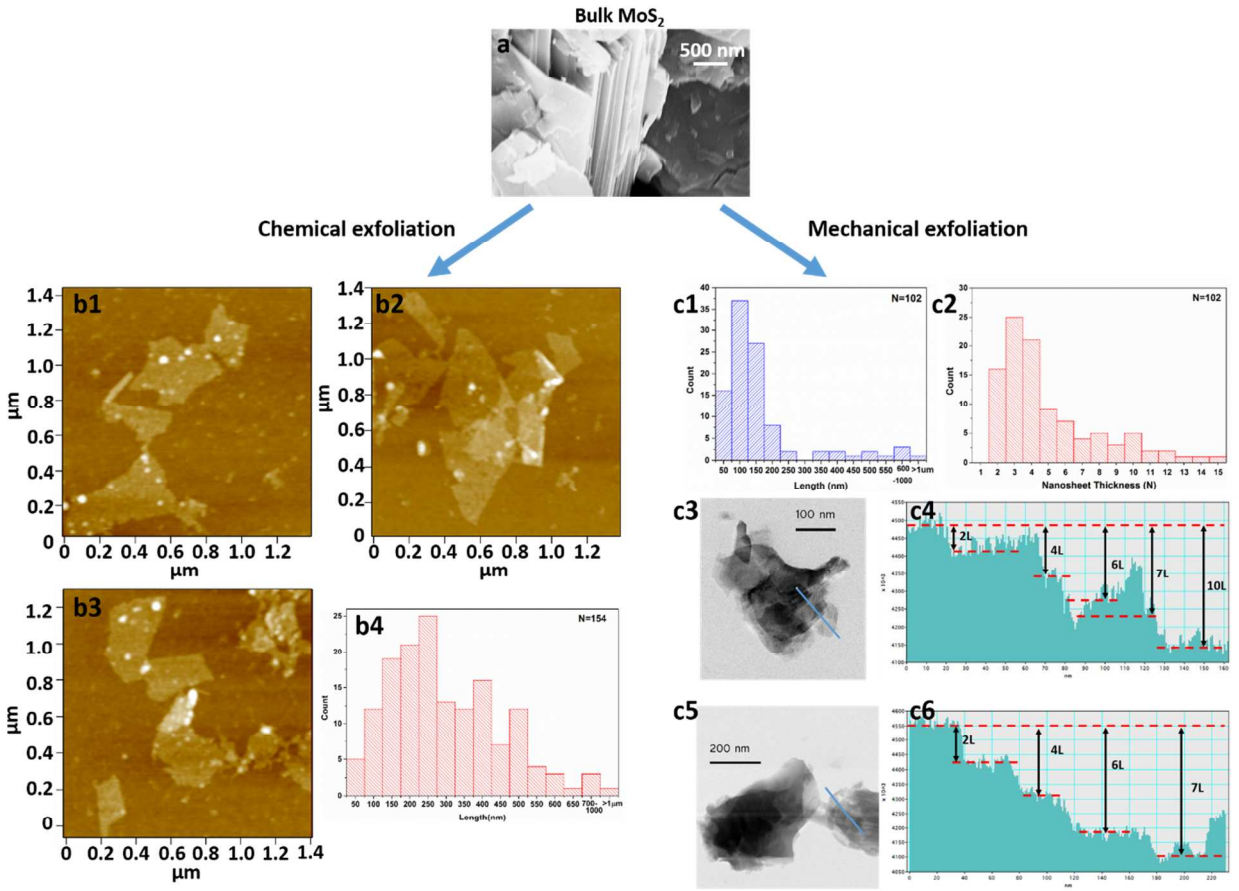

Figure S1. (a) SEM image of bulk and lamellar MoS_2 (~ 2 µm), which is chemically and mechanically exfoliated to ce-MoS_2 and me-MoS_2 nanosheets, respectively. (b1-3) AFM images of ce-MoS_2 showing the dominant monolayer form; (b4) the lateral length histogram of ce-MoS_2, on the basis of measurements on 154 ce-MoS_2 nanosheets. For me-MoS_2 sample, the histogram of nanosheet lateral length (c1) and thickness is based on the measurements of 102 nanosheets. The thickness is estimated by the examination of nanosheet edges described previously.[1] Specifically, on the STEM images of me-MoS_2 nanosheets (c3 and c5), line-scans are performed on the images marked by blue lines, and give the intensity profiles on the right (c4 and c6). The stepwise change of intensity at layer edges can provide an estimation of layer number.

Table S1.Thermodynamic oxidation potential of MoS_2 and $MoSe_2$ in aqueous solution

Calculation of the oxidation potentials of TMDs was based on a method developed previously.[2] To derive the oxidation potential from thermodynamic data, the electrode reaction of the reference (NHE) was added to the Eq. (1) to obtain the net reaction, as in Eq. (2)

$$MX \rightleftharpoons M^{z+} + X + ze^- \text{ (oxidation)} \quad (1)$$

$$MX + zH^+ \rightleftharpoons M^{z+} + X + \frac{z}{2}H_2 \text{ (oxidation)} \quad (2)$$

Consequently, the oxidation potential (relative to NHE) is calculated on the basis of the free energy difference ΔG for the combination of the net reaction, as shown in the Eq. (3).

$$\varphi^{ox} = (G(M^{z+}) + G(X) - G(MX))/zeF \quad (3)$$

where *G* is the standard-state Gibbs free energy, *e* the elementary charge and *F* the Faraday constant. Note that the generic half-reaction shown is a simple example for a non-oxidizable "X". A TMD material is predicted to be thermodynamically unstable if its φ^{ox} value is lower (more negative) than that of the oxidant of interest (here the oxygen/water redox couple $\varphi(O_2/H_2O)$). The dependence of oxidation potential on specific conditions (concentration and pH) can be further examined using the Nernst equation. The Gibbs formation energies of TMDs and soluble ions can be found in property reference handbooks.[3] Multiple oxidation reactions are possible, and each of them will give rise to a slightly different oxidation potential. For MoS_2 and $MoSe_2$, the most likely oxidation reactions and their corresponding oxidation potential are listed below, with value in bold used in the analysis (see Fig. S2).

TMD	Reaction	Potential, V
MoS_2	$MoS_2 + 12H_2O \rightarrow MoO_4^{2-} + 2SO_4^{2-} + 9H_2 + 6H^+$	**0.429**
	$MoS_2 + 4H_2O \rightarrow MoO_4^{2-} + 2S + 3H_2 + 2H^+$	0.5831
$MoSe_2$	$MoSe_2 + 12H_2O \rightarrow MoO_4^{2-} + 2SeO_4^{2-} + 9H_2 + 6H^+$	0.655
	$MoSe_2 + 4H_2O \rightarrow MoO_4^{2-} + 2Se + 3H_2 + 2H^+$	**0.215**

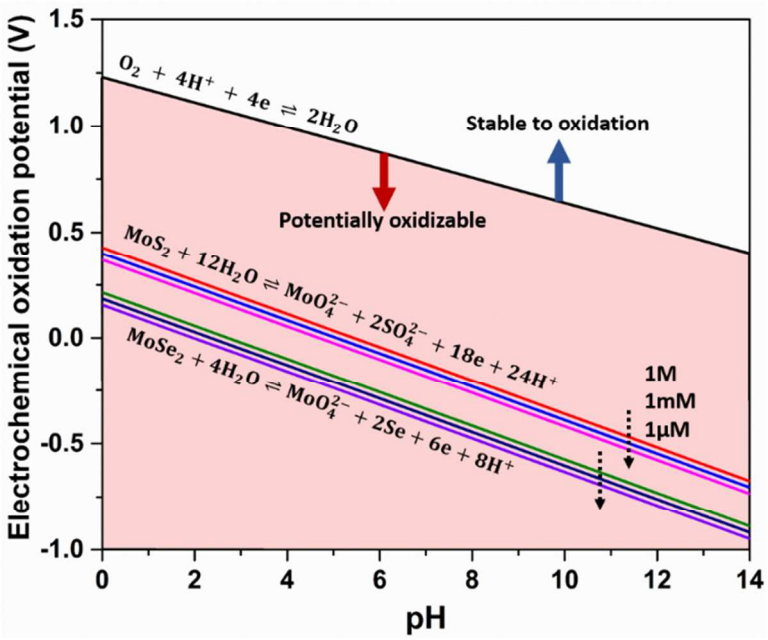

Figure S2. Thermodynamic analysis of layered MoS_2 and $MoSe_2$ oxidation by dissolved O_2 in aqueous media. The pH-dependent redox potential of the O_2/H_2O couple divides the space into two regions: a lower region where material oxidation is thermodynamically favored and an upper region where the materials are thermodynamically stable to oxidation. Both molybdenum dichalcogenides are predicted to be thermodynamically unstable to O_2 oxidation under all pH conditions examined.

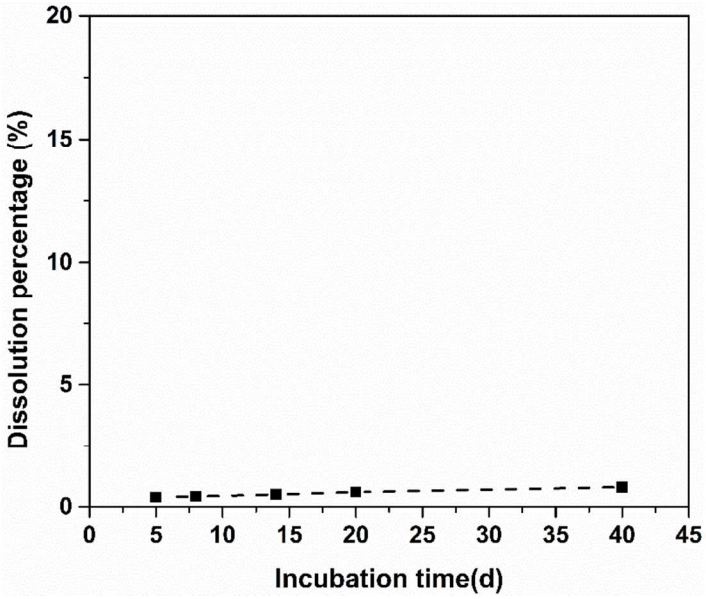

Figure S3. Time-dependent dissolution of bulk MoS_2 (starting concentration 100ppm, size ~2 μm) in HEPES buffer (pH 7.4). The measured concentration is close to the detection limits of ICP-AES (50 ppb).

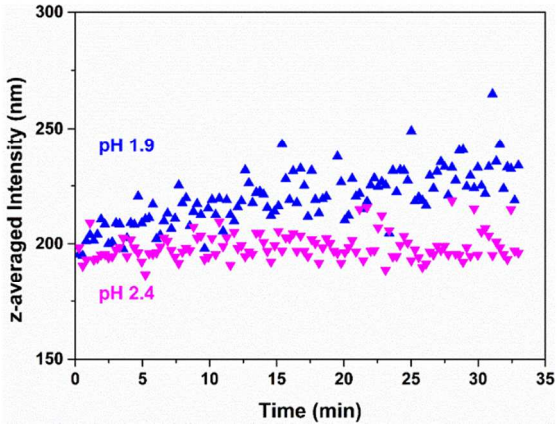

Figure S4. Higher resolution view of DLS measurement of MoS_2 solution (~10 ppm of Mo) at pH ~2, indicating that aggregation begins to occur at pH values around 1.9, but not at 2.4.

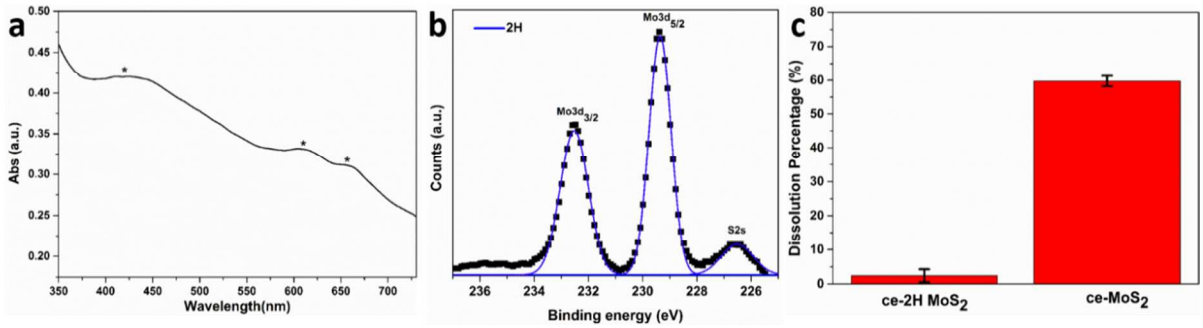

Figure S5. UV-vis spectrum (**a**) and XPS spectrum (**b**) of ce-MoS_2 treated by hydrothermal reaction at 200 °C for 4 hours, both confirming the conversion of 1T to 2H. (**c**) The oxidative dissolution of ce-2H MoS_2 is significantly inhibited compared to that of ce-MoS_2 under the same conditions (1-day incubation in pH 11.2 buffer).

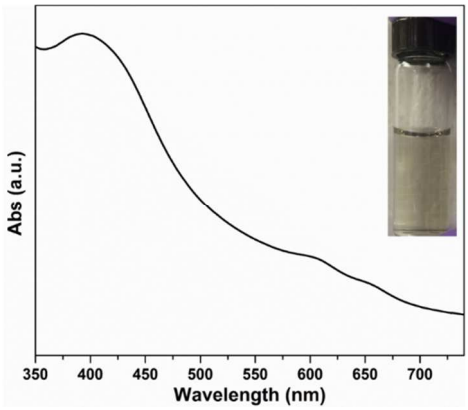

Figure S6. UV-vis spectrum of the low concentration sample (follow-up measurement in Figure 2a) after storage in air for one year. The appearance of characteristic peaks of 2H phase implies 2H phase in the mixed ce-MoS_2 is more strongly resistant to oxidative dissolution, though the overall ce-MoS_2 undergoes significant dissolution (more than 90% of molybdenum exists as soluble Mo). The apparent "persistence"

comes from the low pH conditions in this experiment, and the slow oxidation kinetics of the 2H component in ce-MoS_2 sample.

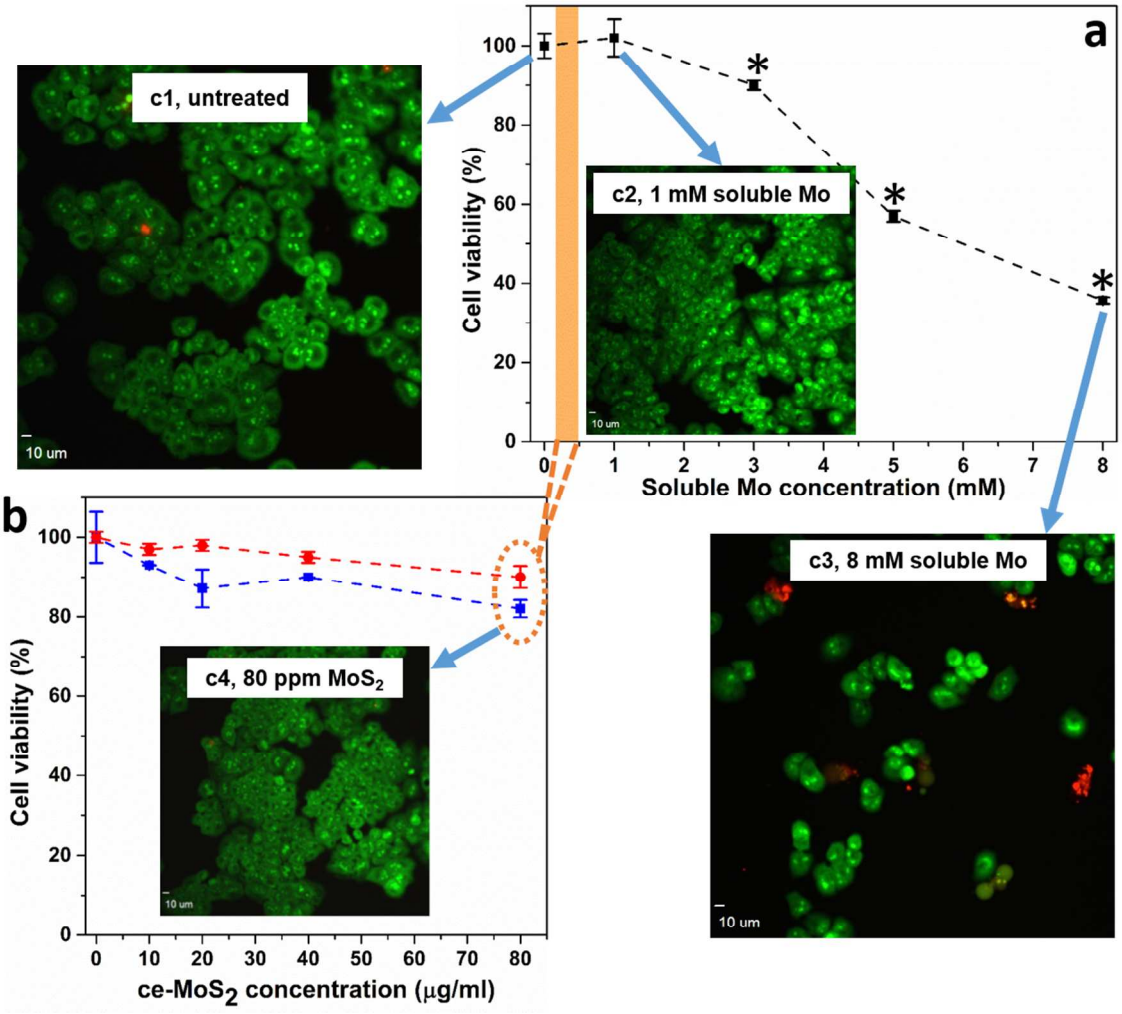

Figure S7. Cytotoxicity to human lung epithelial cells of ce-MoS_2 nanosheets and soluble molybdate ions. Assessment of cell viability after exposure of human lung epithelial cells to different concentrations of Mo salt (a) and ce-MoS_2 sample (b). Following exposure to various amounts of Mo salt for 1 d or ce-MoS_2 samples for 1 (blue trace) or 3 days (red trace), viability was assessed using dehydrogenase activity assay Wst 8. Concentrations above 3 mM Mo salt caused a significant decrease of viability (*$p < 0.05$). There was no significant cell death measured for nanosheet samples within 3 days of treatment. Images show visualization of cell death in epithelial cells using ethidium homodimer/Syto 10 stain after exposure to Mo salt or ce-MoS_2 nanosheets for 24 hours. Epithelial cells were seeded into 96 well plates and imaged using an Olympus confocal microscope to visualize live (green) and dead (red) cells. Cells exposed to 8 mM Mo salt (c3) show strong red fluorescence and significant loss in cell count, while unexposed cells (c1), cells exposed to 1 mM Mo salt (c2), 80 μg/ml MoS_2 nanosheets (c4) do not show toxicity, shown by strong green fluorescence.

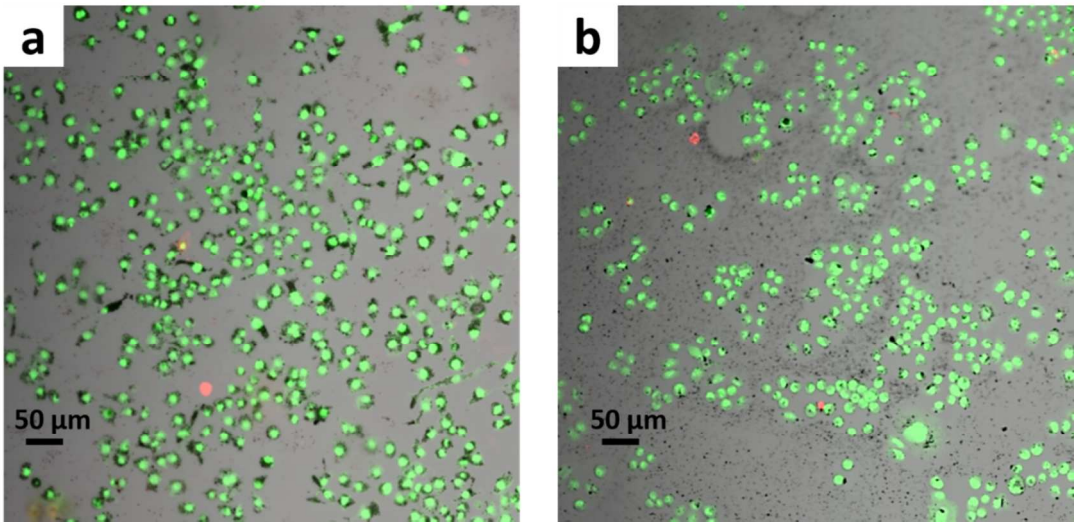

Figure S8. Visualization of cell death and uptake of MoS_2 in murine macrophages and human lung epithelial cells was conducted using ethidium-homodimer /Syto 10 stain after exposure to to 80 µg/mL MoS_2 for 24 hours. Cells were washed once and incubated with 5 µM/ml Syto10/ and 1 µg/ml ethidium homodimer (Invitrogen) in phosphate buffered saline for 5 min (macrophages) or 15 min (lung epithelial cells). Images were visualized using a spinning-disk Olympus confocal fluorescence (Model IX81) motorized inverted research microscope using brightfield and fluorescence filter system.

Reference

1. Smith, R. J.; King, P. J.; Lotya, M.; Wirtz, C.; Khan, U.; De, S.; O'Neill, A.; Duesberg, G. S.; Grunlan, J. C.; Moriarty, G. Large-Scale Exfoliation of Inorganic Layered Compounds in Aqueous Surfactant Solutions. *Adv. Mater.* **2011**, 23, 3944-3948.
2. Chen, S.; Wang, L.-W. Thermodynamic Oxidation and Reduction Potentials of Photocatalytic Semiconductors in Aqueous Solution. *Chem. Mater.* **2012**, 24, 3659-3666.
3. Haynes, W. M. *CRC handbook of chemistry and physics*. CRC press: **2014**.